Research Article Vol. 6, No. 5 / May 2019 / Optica 557

2D broadband beamsteering with large-scale MEMS optical phased array

Youmin Wang,[1] Guangya Zhou,[2] Xiaosheng Zhang,[1] Kyungmok Kwon,[1] Pierre-A. Blanche,[3] Nicholas Triesault,[4] Kyoung-sik Yu,[5] and Ming C. Wu[1,*]

[1]Department of Electrical Engineering and Computer Sciences, University of California, Berkeley, California 94720, USA
[2]Department of Mechanical Engineering, National University of Singapore, 9 Engineering Drive 1, Singapore
[3]College of Optical Sciences, The University of Arizona, Tucson, Arizona 85721, USA
[4]Independent Researcher, Santa Clara, California 95050, USA
[5]School of Electrical Engineering, Korea Advanced Institute of Science & Technology (KAIST), 291 Daehak-ro, Yuseong-gu, Daejeon, South Korea
*Corresponding author: mingwu@berkeley.edu

Received 29 October 2018; revised 20 March 2019; accepted 1 April 2019 (Doc. ID 349340); published 29 April 2019

Optical-phased arrays (OPAs) enable complex beamforming, random-access beam pointing, and simultaneous scan and tracking of multiple targets by controlling the phases of two-dimensional (2D) coherent emitters. So far, no OPA can achieve all desirable features including large 2D arrays, high optical efficiency, wideband operation in wavelengths, fast response time, and large steering angles at the same time. Here, we report on a large-scale 2D OPA with novel micro-electro-mechanical-system (MEMS)-actuated phase shifters. Wavelength-independent phase shifts are realized by physically moving a grating element in the lateral direction. The OPA has 160 × 160 independent phase shifters across an aperture of 3.1 mm × 3.2 mm. It has a measured beam divergence of 0.042° × 0.031°, a field of view (FOV) of 6.6° × 4.4°, and a response time of 5.7 μs. It is capable of providing about 25,600 rapidly steerable spots within its FOV. The grating phase shifters are optimized for the near-infrared telecom wavelength bands from 1200 to 1700 nm with 85% optical efficiency.

https://doi.org/10.1364/OPTICA.6.000557

1. INTRODUCTION

Optical-phased arrays (OPAs) enable electronic steering of optical beams. By customizing the optical phases of individual emitters in a two-dimensional (2D) array, versatile beamforming functions such as random-access beam pointing, independent scanning of multiple beams, and simultaneous scanning and tracking of targets can be realized, similar to the phased-array radars or synthetic apertures in the microwave regime. They are compact, robust, agile, and can be scaled to large apertures for longer reach. They have wide applications including light detection and ranging (LiDAR) [1–3], free-space optical communications (FSOC) [4], optical switches [5,6], holographic displays [7,8], and three-dimensional brain imaging [9]. One-dimensional (1D) OPAs have been formed by integrating phase modulators in linear arrays of waveguides. They were first reported in lithium tantalite [10] and GaAs [11] waveguides and recently extended to silicon photonic-integrated circuits [12–14], in which pixel-wise modulation of phase and amplitude is possible [14]. Scanning in the second axis was achieved by using a widely tunable laser source in conjunction with grating couplers. However, it does not have the benefits of OPA. Moreover, the association of beam-pointing direction with wavelength is not desirable for coherent FSOC, optical switching, holographic display, or optogenetics. Some 2D silicon photonic OPAs have been reported; however, they are limited to small arrays (8 × 8) [2,14,15]. A large array is important for many OPA applications because the number of resolvable spots in the far field is approximately equal to the number of phase shifters in the OPA. For example, automotive LiDAR requires hundreds to thousands of resolvable spots in the horizontal direction.

2D OPAs are currently available in liquid crystal-on-silicon (LCOS) spatial light modulators [16–18]. Liquid crystal is birefringent, and its optical refractive index can be changed by an electric field [19]. By integrating liquid crystals directly on complementary metal-oxide-semiconductor (CMOS) drivers, 2D-OPA with a very large number of pixels (8 million) has been realized [20]. Initially developed for microdisplay and digital projectors, LCOS is also used for fiber-optic switches [6] and holographic optogenetics [9]. A main drawback of LCOS is its slow response time (~milliseconds) due to the viscoelasticity of the fluid that slows down the reorientation of molecules [19]. This is far too slow for LiDAR, FSOC, and fast optical switches.

Faster 2D OPA with microsecond response time can be realized with microelectro-mechanical-system (MEMS) actuation. Typically, MEMS OPA comprises micromirrors on "piston" actuators that move vertically. The phase of the reflected wave experiences a 2π phase shift when the mirror is displaced by half a wavelength [21]. 2D MEMS OPAs have been reported for UV [22,23] and near-infrared wavelengths [24–27]. In addition to fast response time, MEMS OPAs are capable of withstanding high optical power and polarization-independent operation. The main

challenge of piston mirrors is the large displacement (half wavelength) required to achieve a 2π phase shift, particularly at long wavelength. The electrostatic pull-in effect limits the usable displacement to 1/3 of the gaps in parallel-plate actuators [28]. This leads to high voltage operation and increased crosstalk among adjacent pixels.

In this paper, we report on a large-scale 2D OPA with novel MEMS-actuated grating phase shifters. By moving a grating element laterally, the optical phase of the diffracted beam is shifted in proportion to the displacement [29]. Unlike piston mirrors, this phase shift is independent of wavelength, which enables broadband applications without loss of efficiency. Previously, a 1D OPA with 24 phase shifters was reported [29]. Here, we extended the OPA to large 2D arrays with 160 × 160 phase shifters, greatly reducing the beam divergence and increasing the number of resolvable spots. High fill factor, high optical efficiency, and large field-of-view were achieved by stacking fine-pitched grating phase shifters on top of MEMS actuators. A detailed comparison of our work and reported OPAs is summarized in Table S1 of Supplement 1.

2. DESIGN OF GRATING-BASED MEMS PHASE SHIFTERS

The proposed OPA is based on a novel phase shifter first reported by Zhou *et al.* [29]. The phase shifter consists of a diffraction grating with free-space input and output beams, as shown in Fig. 1. The grating is physically movable along the grating-vector direction in the plane of the array. The lateral motion ensures a flat optical surface for any phase map, avoiding the shadowing effect in piston mirrors. The diffraction angle is not affected by the movement of the grating. However, the optical phase of the first-diffraction-order beam is shifted in proportion to the displacement: $\Delta\phi = 2\pi\Delta x/\Lambda$, where Δx is the lateral displacement, and Λ is the grating period [29]. A detailed derivation of the phase shift is presented in Supplement 1. Note that this phase shift is independent of wavelength, unlike piston mirrors or other commonly used phase shifters. The same phase map can be used for a broad range of wavelengths, enabling control of multiple beams with different wavelengths, although the angular position of the diffracted pattern will change as the first-order-diffracted beam direction is dependent on the wavelength of the input beam. The OPA consists of a 2D array of individually addressable-grating phase shifters (Fig. 1). The grating lines of all phase shifters are initially aligned such that the whole array operates as a single grating. To steer or synthesize complex output beams, each grating element is individually displaced to achieve the desired phase map.

To test the feasibility of this new OPA concept, we first fabricated fixed-grating arrays with predetermined offsets among the grating elements. Figure 2(a) shows the scanning electron micrograph (SEM) of a grating array corresponding to a hologram of the "Cal" logo. We have used an array with 320 × 320 grating elements for both simulation and experimental verification. The grating elements have a 10 μm pitch and a grating period of 1 μm. Figure 2(b) shows the measured far-field pattern of the first-order-diffraction beam. The Cal feature is faithfully reproduced with good agreement with the simulations in Fig. 2(c). The optical contrast of the diffracted hologram, defined as the ratio of the intensity distributed within the desired pattern versus the overall intensity of the outgoing beam from the grating-element array, is measured to be 87.7% [Fig. 2(b)]. The desired

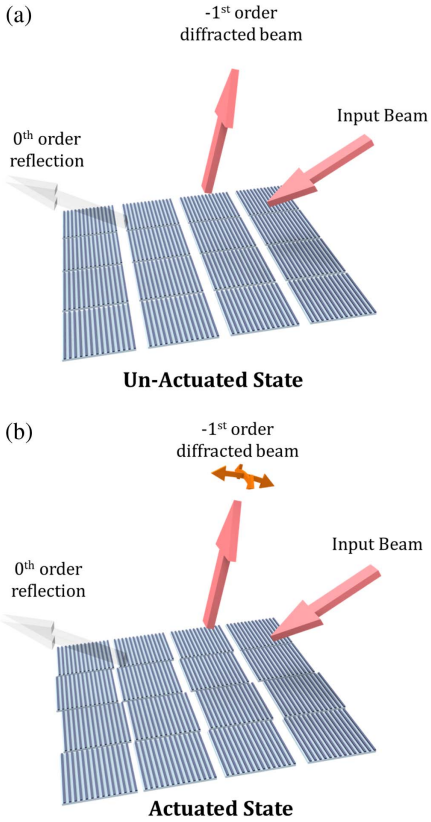

Fig. 1. MEMS grating OPA working principle: (a) schematic of the grating-based 2D OPA without actuation. All grating phase-shifting elements are aligned to form a large continuous grating. Light is incident at a shallow angle (65°). The grating profile is designed to maximize the efficiency of the first-order-diffraction beam and minimize the reflection beam. (b) To steer the optical beam, the grating elements are moved individually to produce the desired phase map for the output beam.

phase shift of individual grating elements was determined by the Gerchberg–Saxton algorithm. The classic Gerchberg–Saxton algorithm used here still renders intensity inhomogeneity of the diffracted pattern. The modified Gerchberg–Saxton algorithm [30,31] could improve the efficiency and homogeneity; however, this is beyond the scope of this work. This experiment demonstrates the feasibility of using grating-phase shifters for OPAs.

To enable dynamically reconfigurable OPA, we integrate a MEMS actuator with each phase shifter to move it along the grating vector direction. Combdrive actuators are ideal for this purpose because they are capable of large displacement without suffering from the pull-in effect [32]. We used a grating period of 955 nm so a phase shift of 2π is realized with a displacement of 955 nm, well within the range of our combdrive actuators. The resulting 2D OPA is shown in Fig. 3. The gratings have been optimized for high diffraction efficiency from 1200 to 1700 nm [Supplement 1, Fig. S2]. The optical beam is incident at 65° from the surface normal, and the output beam from the first-order diffraction is directed at 45°.

The key specifications of an OPA include its pitch, aperture size, and the number of elements in the array. Ideally, the pitch should be minimized to achieve a large FOV. At the same time, each pixel must accommodate a MEMS actuator and mechanical spring for a fully programmable OPA. The pitches of the OPA in this work are 19.1 and 20 μm in the X and Y axes, respectively. Considering the 45° output angle with respect to the grating normal direction, the

effective pitch sizes are 13.5 and 20 μm. The largest steerable angles of the MEMS grating OPA at 1550 nm are

$$\theta_x = \pm \arcsin\left(\frac{\lambda}{2\Lambda_x}\right) = \pm 3.29°,$$
$$\theta_y = \pm \arcsin\left(\frac{\lambda}{2\Lambda_y}\right) = \pm 2.22°. \quad (1)$$

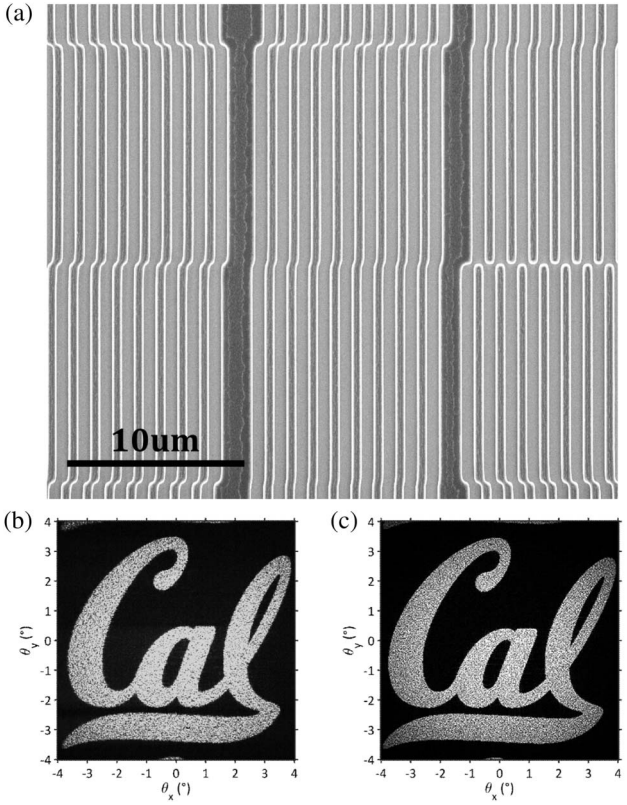

Fig. 2. (a) SEM of a static grating phase shifter array to generate the "Cal" logo; (b) measured and (c) simulated far-field patterns of the first-order diffraction beam.

Here $\lambda = 1550$ nm is the operating wavelength, and $\mathbf{\Lambda}_x$ and $\mathbf{\Lambda}_y$ are the effective pitches in the X and Y directions, respectively. The OPA has 160 × 160 phase shifters, forming an optical aperture of 3.1 mm × 3.2 mm. The theoretical divergence angle is determined by λ/D, where D is the effective aperture size. The effective aperture size for the output beam is reduced to 2.2 mm × 3.2 mm due to the angled incident and diffraction directions. This rectangular aperture will produce an output beam with a theoretical divergence angle of 0.040° × 0.027° when illuminated with a uniform intensity. To our knowledge, this is the largest chip-scale OPA device with microsecond response time.

To increase the fill factor, the combdrive actuator is integrated underneath the grating element, as shown in Fig. 3. The combdrive actuator in our design is bidirectional, with up to 1 μm displacement in either direction. The grating is attached to the movable comb, which is tethered to the anchor point through two folded springs. A phase shift of $\pm\pi$ is obtained with a ±477.5 nm displacement. To increase the actuation force and reduce the operating voltage, we use deep-UV lithography to pattern combs with 300 nm fingers and 300 nm spacings. This increases the number of gaps in the combdrive (32) and the actuation force (0.21 μN at 10.5 V). Similarly, we also use narrow (300 nm) springs to lower the actuation voltage (10.5 V). Even with this spring constant, we are able to achieve a high resonance frequency of 55 kHz, thanks to the small mass of the grating pixel. This is sufficient to achieve microsecond response time for the optical phased array.

3. EXPERIMENTAL RESULTS

The 2D MEMS OPA has been fabricated using an eight-mask surface-micromachining process with polysilicon as structural materials. The detailed fabrication process is shown in Supplement 1, Fig. S3. The photograph of the OPA chip is shown in Fig. 4(a) with a U.S. quarter coin in the background. Figure 4(b) shows the confocal optical micrograph of the 5 mm × 5 mm chip obtained by Olympus LEXT OLS3000 3D laser confocal microscope. The optical aperture formed by 160 × 160 phase shifters is 3.1 mm × 3.2 mm. The SEM of the fabricated OPA is shown

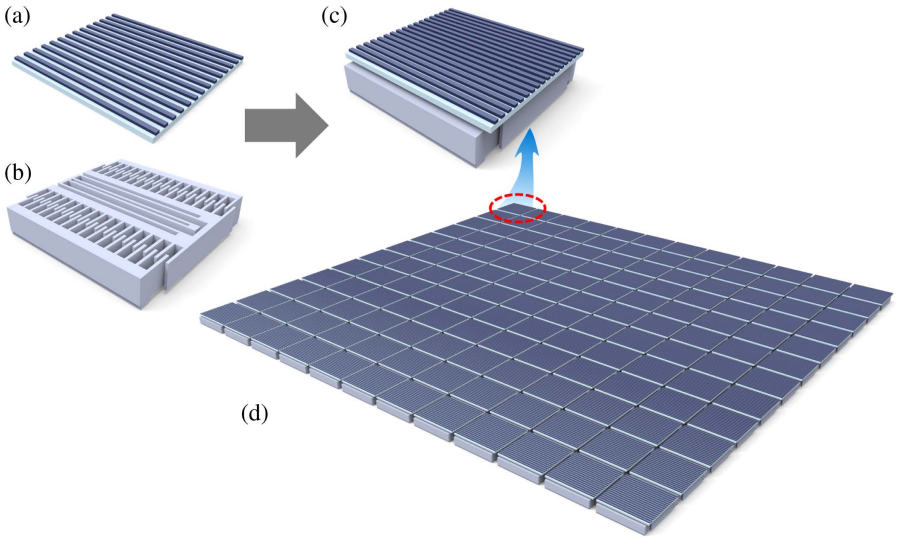

Fig. 3. MEMS grating OPA schematic: (a) top grating layer of the MEMS OPA; (b) bottom lateral combdrive structure; (c) integrated MEMS OPA phase-shifting element with grating and MEMS actuator; and (d) 2D MEMS grating OPA composed of an array of identical active phase-shifting elements.

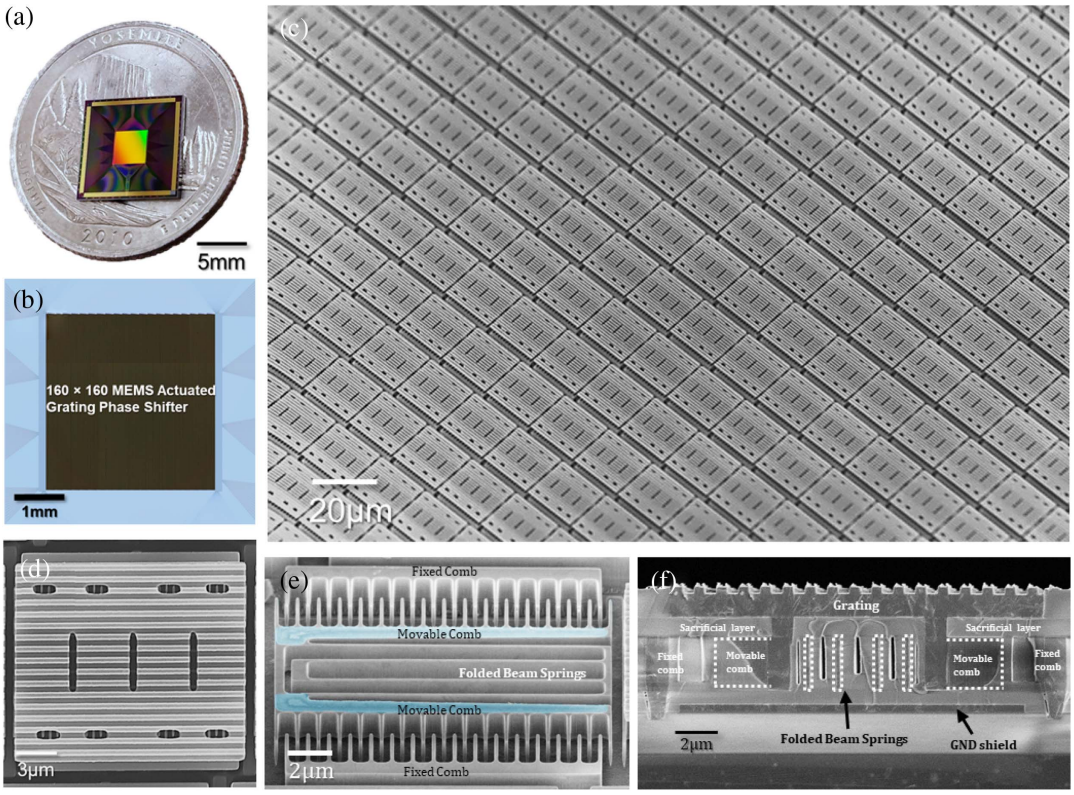

Fig. 4. Fabricated 2D MEMS grating OPA: (a) photograph of the OPA on a U.S. quarter coin; (b) confocal optical micrograph showing the optical aperture; (c) scanning electron microscope (SEM) image of the OPA; (d) close-up view of a single MEMS grating element; (e) hidden combdrive actuator underneath the grating. The grating is attached to the blue-shaded movable comb beams; and (f) cross-sectional SEM of an OPA element before HF release.

in Fig. 4(c). The close-up view of a phase shifter in Fig. 4(d) clearly shows the grating structure. Release holes are etched on the grating to facilitate wet HF release of the MEMS structures. The combdrive actuator element is shown in Fig. 4(e). High fill factor (84.7%) is achieved by hiding the combdrive actuator underneath the grating. The maximum range of the combdrive is limited to 1 μm by a mechanical stopper to prevent electrical short circuit.

The electrical interconnect lines are routed underneath the pixels to fit in the tight pitch of the OPA. The cross-sectional SEM of a phase shifter [Fig. 4(f)] clearly shows the vertically stacked structures with gratings on top of MEMS actuators and the interconnect lines. A ground plane is inserted between the actuator and the interconnect lines to eliminate electrical crosstalk. Only the fixed combs are biased. The movable combs are grounded, along with the gratings and the mechanical springs.

The fabricated OPA chip is wirebonded to a printed circuit board (PCB) for electrical and optical testing. To achieve $\pm\pi$ phase shift, 10.5 V actuation voltage is applied to move the OPA pixel by ±0.5 μm in the lateral direction (Supplement 1, Fig. S4). This low actuation voltage is amenable to integration with CMOS electronic drivers. The frequency response of the grating phase shifter is characterized by a Lyncée Tec digital holographic microscope (Visualization 1). The resonance frequency is 55 kHz, corresponding to a rise time of 5.7 μs for a π phase shift (Supplement 1, Figs. S5 and S6).

We have performed beamsteering experiments with various phase maps using a laser source at 1550 nm wavelength. An optical setup (Supplement 1, Fig. S7a) was built to capture the far-field patterns by a Xenics Bobcat-320 InGaAs IR camera. Figures S7(b) and S7(c) of Supplement 1 show the measured beam profile with 0.042° × 0.031° divergence angle. Figure 5(a) shows the overlay of all the steered angles within the 6.6° × 4.4° FOV. Due to the limited number of addressing pin-count (256 in our case), the total number of steerable spots in the far-field is restricted to 9 × 17. Because every OPA element takes two pins, the array is grouped into 8 × 16 subarrays, within which every phase shifter is independently addressed. The corresponding phase shifters in different subarrays are connected on chip to reduce the pin count. Figure 5(b) shows the measured main-to-sidelobe suppression ratio (MSSR) of the steered lobe in the FOV over all the angles. Figure 5(c) shows five different beam steering profiles in 3D and waterfall styles (Visualization 2 and Visualization 3), pointing at angles of (0°, 0°), (−2.47°, 0.83°), (2.47°, −0.83°), (−0.82°, 1.39°), and (0.82°, −1.39°). The MSSR of these steered beams are 17.7, 14.0, 12.4, 10.8, and 14.8 dB, respectively. In this measurement, uncoated silicon gratings are used in our OPA with an optical efficiency of 16%. Metal coating can further increase the diffraction efficiency (Supplement 1, Fig. S2).

Due to the pin-count limit, we can only access 9 × 17 angles in the current OPA. The output beams are diffraction limited and can fully support the theoretical number of resolvable spots of 160 × 160. To overcome the pin-count limit, the MEMS OPA can be fabricated on a CMOS wafers to integrate the addressing electronics, as demonstrated in commercial digital light processing (DLP) projectors [33] and micromirror arrays for wavefront control [34]. Lower temperature MEMS materials such as

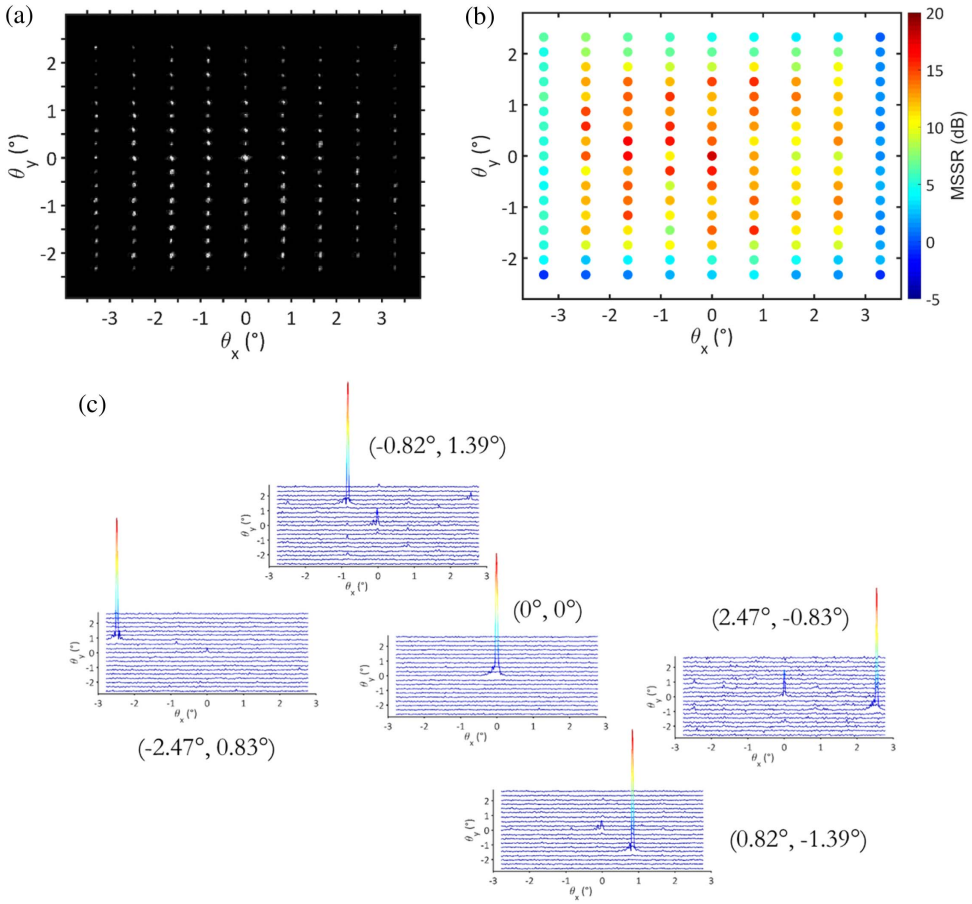

Fig. 5. Beamsteering results: (a) overlay of steered beams within the FOV; (b) measured main-to-sidelobe suppression ratio (MSSR) of the steered beam spots; and (c) waterfall images showing beam profiles at different angles.

low-stress metals [33,34] or polycrystalline silicon-germaniums [35] are compatible with postprocessing of CMOS wafers.

According to Bragg's law the beamsteering angle of the OPA can be changed by adjusting the incident beam wavelength (Visualization 4), the FOV of the OPA can be increased by reducing the pixel size. To test the optical performance, we have fabricated holographic images on phase grating elements with pitches of 3, 5, 10, and 20 μm (Supplement 1, Fig. S10). Excellent image qualities have been obtained for all pitches. The OPA with 3 μm would have an FOV of 26.7° × 24.8° at 1260 nm wavelength. The main challenge is the scaling of the mechanical springs. Indeed, the spring constant is proportional to the cube of the ratio between the spring length and the spring width. To compensate for the reduction of spring length, the spring width needs to shrink proportionally. The sidewall spacer process can produce springs as narrow as a few tens of nm [36]. This process can potentially produce OPAs with larger FOVs.

4. CONCLUSIONS

We have designed and experimentally demonstrated a 2D MEMS optical phased array with 25,600 phase shifters over an aperture of 3.1 mm × 3.2 mm. The field of view for the OPA is 6.6° × 4.4° at 1550 nm wavelength. A displacement of ±0.5 μm is measured at 10.5 V, corresponding to a wavelength-independent phase shift of $\pm\pi$. Two-dimensional beamsteering and holographic beam forming have been successfully demonstrated. The MEMS OPA has a resonance frequency of 55 kHz which corresponds to a response time of 5.7 μs.

Funding. Berkeley Sensor and Actuator Center (BSAC); National Science Foundation (NSF) (1640329); Texas Instruments (TI); Huawei Technologies; Industrial Technology Research Institute (ITRI).

See Supplement 1 for supporting content.

REFERENCES

1. J. Levinson, J. Askeland, J. Becker, J. Dolson, D. Held, S. Kammel, J. Z. Kolter, D. Langer, O. Pink, V. Pratt, and M. Sokolsky, "Towards fully autonomous driving: systems and algorithms," in *IEEE Intelligent Vehicles Symposium (IV)* (2011), pp. 163–168.
2. R. Fatemi, B. Abiri, and A. Hajimiri, "An 8 × 8 heterodyne lens-less OPA camera," in *Conference on Lasers and Electro-Optics*, San Jose, California, 2017, p. JW2A.9.
3. C. V. Poulton, A. Yaacobi, D. B. Cole, M. J. Byrd, M. Raval, D. Vermeulen, and M. R. Watts, "Coherent solid-state LIDAR with silicon photonic optical phased arrays," Opt. Lett. **42**, 4091–4094 (2017).
4. W. M. Neubert, K. H. Kudielka, W. R. Leeb, and A. L. Scholtz, "Experimental demonstration of an optical phased array antenna for laser space communications," Appl. Opt. **33**, 3820–3830 (1994).
5. P.-A. Blanche, L. LaComb, Y. Wang, and M. C. Wu, "Diffraction-based optical switching with MEMS," Appl. Sci. **7**, 411 (2017).
6. S. Frisken, G. Baxter, D. Abakoumov, H. Zhou, I. Clarke, and S. Poole, "Flexible and grid-less wavelength selective switch using LCOS

technology," in *Optical Fiber Communication Conference and Exposition and the National Fiber Optic Engineers Conference* (2011), pp. 1–3.
7. E. L. Pearson, "MEMS spatial light modulator for holographic displays," Thesis (Massachusetts Institute of Technology, 2001).
8. M. Stanley, M. A. G. Smith, A. P. Smith, P. J. Watson, S. D. Coomber, C. D. Cameron, C. W. Slinger, and A. Wood, "3D electronic holography display system using a 100-megapixel spatial light modulator," presented at the Optical Systems Design, St. Etienne, France, 2004, p. 297.
9. N. C. Pégard, A. R. Mardinly, I. A. Oldenburg, S. Sridharan, L. Waller, and H. Adesnik, "Three-dimensional scanless holographic optogenetics with temporal focusing (3D-SHOT)," Nat. Commun. **8**, 1228 (2017).
10. R. A. Meyer, "Optical beam steering using a multichannel lithium tantalate crystal," Appl. Opt. **11**, 613–616 (1972).
11. F. Vasey, F. K. Reinhart, R. Houdré, and J. M. Stauffer, "Spatial optical beam steering with an AlGaAs integrated phased array," Appl. Opt. **32**, 3220–3232 (1993).
12. C. V. Poulton, M. J. Byrd, M. Raval, Z. Su, N. Li, E. Timurdogan, D. Coolbaugh, D. Vermeulen, and M. R. Watts, "Large-scale silicon nitride nanophotonic phased arrays at infrared and visible wavelengths," Opt. Lett. **42**, 21–24 (2017).
13. D. N. Hutchison, J. Sun, J. K. Doylend, R. Kumar, J. Heck, W. Kim, C. T. Phare, A. Feshali, and H. Rong, "High-resolution aliasing-free optical beam steering," Optica **3**, 887–890 (2016).
14. H. Abediasl and H. Hashemi, "Monolithic optical phased-array transceiver in a standard SOI CMOS process," Opt. Express **23**, 6509–6519 (2015).
15. J. Sun, E. S. Hosseini, A. Yaacobi, D. B. Cole, G. Leake, D. Coolbaugh, and M. R. Watts, "Two-dimensional apodized silicon photonic phased arrays," Opt. Lett. **39**, 367–370 (2014).
16. P. F. McManamon, T. A. Dorschner, D. L. Corkum, L. J. Friedman, D. S. Hobbs, M. Holz, S. Liberman, H. Q. Nguyen, D. P. Resler, R. C. Sharp, and E. A. Watson, "Optical phased array technology," Proc. IEEE **84**, 268–298 (1996).
17. P. F. McManamon, P. J. Bos, M. J. Escuti, J. Heikenfeld, S. Serati, H. Xie, and E. A. Watson, "A review of phased array steering for narrowband electrooptical systems," Proc. IEEE **97**, 1078–1096 (2009).
18. D. P. Resler, D. S. Hobbs, R. C. Sharp, L. J. Friedman, and T. A. Dorschner, "High-efficiency liquid-crystal optical phased-array beam steering," Opt. Lett. **21**, 689–691 (1996).
19. Z. Zhang, Z. You, and D. Chu, "Fundamentals of phase-only liquid crystal on silicon (LCOS) devices," Light: Sci. Appl. **3**, e213 (2014).
20. S. Hashimoto, O. Akimoto, H. Ishikawa, T. Kiyomiya, T. Togawa, T. Isozaki, H. Abe, M. Nakai, H. Terakawa, H. Horikiri, T. Ishii, and M. Kogure, "39.2: SXRD (Silicon X-tal reflective display); a new display device for projection displays," SID Symp. Dig. Tech. Pap. **36**, 1362–1365 (2005).
21. T.-H. Lin, "Implementation and characterization of a flexure-beam micromechanical spatial light modulator," Opt. Eng. **33**, 3643–3648 (1994).
22. M. Hacker, G. Stobrawa, R. Sauerbrey, T. Buckup, M. Motzkus, M. Wildenhain, and A. Gehner, "Micromirror SLM for femtosecond pulse shaping in the ultraviolet," Appl. Phys. B **76**, 711–714 (2003).
23. D. Lopez, V. Aksyuk, G. Watson, M. E. Simon, W. Mansfield, F. Klemens, R. Cirelli, E. Ferry, A. Papazian, F. Pardo, C. Bolle, N. Basavanhally, J. Bower, J. Miner, T. Sorsch, and D. Tennan, *Two-Dimensional MEMS Piston Array for DUV Optical Pattern Generation* (IEEE, 2006), pp. 148–149.
24. B.-W. Yoo, M. Megens, T. Sun, W. Yang, C. J. Chang-Hasnain, D. A. Horsley, and M. C. Wu, "A 32 × 32 optical phased array using polysilicon subwavelength high-contrast-grating mirrors," Opt. Express **22**, 19029–19039 (2014).
25. W. Yang, T. Sun, Y. Rao, M. Megens, T. Chan, B.-W. Yoo, D. A. Horsley, M. C. Wu, and C. J. Chang-Hasnain, "High speed optical phased array using high contrast grating all-pass filters," Opt. Express **22**, 20038–20044 (2014).
26. T. K. Chan, M. Megens, B.-W. Yoo, J. Wyras, C. J. Chang-Hasnain, M. C. Wu, and D. A. Horsley, "Optical beamsteering using an 8 × 8 MEMS phased array with closed-loop interferometric phase control," Opt. Express **21**, 2807–2815 (2013).
27. B.-W. Yoo, M. Megens, T. Chan, T. Sun, W. Yang, C. J. Chang-Hasnain, D. A. Horsley, and M. C. Wu, "Optical phased array using high contrast gratings for two-dimensional beamforming and beamsteering," Opt. Express **21**, 12238–12248 (2013).
28. W.-M. Zhang, H. Yan, Z.-K. Peng, and G. Meng, "Electrostatic pull-in instability in MEMS/NEMS: a review," Sens. Actuators A, Phys. **214**, 187–218 (2014).
29. G. Zhou and F. S. Chau, "Nondispersive optical phase shifter array using microelectromechanical systems based gratings," Opt. Express **15**, 10958–10963 (2007).
30. S. P. Poland, N. Krstajić, R. D. Knight, R. K. Henderson, and S. M. Ameer-Beg, "Development of a doubly weighted Gerchberg–Saxton algorithm for use in multibeam imaging applications," Opt. Lett. **39**, 2431–2434 (2014).
31. R. D. Leonardo, F. Ianni, and G. Ruocco, "Computer generation of optimal holograms for optical trap arrays," Opt. Express **15**, 1913–1922 (2007).
32. W. C. Tang, T.-C. H. Nguyen, and R. T. Howe, "Laterally driven polysilicon resonant microstructures," Sens. Actuators **20**, 25–32 (1989).
33. L. J. Hornbeck, "Digital light processing for high-brightness high-resolution applications," presented at the Electronic Imaging, San Jose, CA, 1997, pp. 27–40.
34. A. Gehner, P. Durr, D. Kunze, D. Rudloff, A. Elgner, J. Heber, S. Frances, C. Skupsch, H. Torlee, M. Eckert, M. Friedrichs, J. U. Schmidt, W. Pufe, S. Döring, C. Hohle, M. Schulze, and M. Wagner, "Novel 512 × 320 tip-tilt micro mirror array in a CMOS-integrated, scalable process technology," in *International Conference on Optical MEMS and Nanophotonics (OMN)*, 2018, pp. 1–2.
35. A. E. Franke, D. Bilic, D. T. Chang, P. T. Jones, T.-J. King, R. T. Howe, and G. C. Johnson, "Post-CMOS integration of germanium microstructures," in *12th International Conference on Micro Electro Mechanical Systems*, Technical Digest, Orlando, Florida, USA, (IEEE, 1999), pp. 630–637.
36. T. Brosnihan, R. Payne, J. Gandhi, S. Lewis, L. Steyn, M. Halfman, and N. Hagood, "Pixtronix digital micro-shutter display technology: a MEMS display for low power mobile multimedia displays," presented at the MOEMS-MEMS, San Francisco, California, 2010, p. 759408.